

Spiro-Configured Bipolar Host Materials for Highly Efficient Electrophosphorescent Devices

Sung-Yu Ku,^[a] Wen-Yi Hung,^{*[b]} Chung-Wen Chen,^[b] Shih-Wei Yang,^[b] Ejabul Mondal,^[a] Yun Chi,^[c] and Ken-Tsung Wong^{*[a]}

Abstract: In this study, we synthesized and characterized a series of spirobi-fluorene-based bipolar compounds (D2ACN, DNPACN, DNTACN, and DCzACN) in which a dicyano-substituted biphenyl branch, linked orthogonally to a donor biphenyl branch bearing various diarylamines, acted as an acceptor unit allowing fine-tuning of the morphological stability, triplet energy, bipolar transport behavior, and the HOMO and LUMO energy levels. The promising physical properties of these new compounds, together with

their ability to transport electrons and holes with balanced mobilities, made them suitable for use as host materials in highly efficient phosphorescent organic light-emitting diodes (PhOLEDs) with green iridium-based- or red osmium-based phosphors as the emitting layer (EML). We adopted a multi-layer structure to efficiently confine

Keywords: bipolar host • electrophosphorescence • oleds • osmium • spiro compounds

holes and electrons within the EML, thus preventing exciton diffusion and improving device efficiency. The device incorporating D2ACN doped with the red emitter [Os(bpftz)₂(PPhMe₂)₂] (bpftz = 3-(trifluoromethyl)-5-(4-*tert*-butylpyridyl)-1,2,4-triazolate) gave a saturated red electrophosphorescence with CIE coordinates of (0.65, 0.35) and remarkably high efficiencies of 20.3% (21 cd A⁻¹) and 13.5 Lm W⁻¹ at a practical brightness of 1000 cd m⁻².

Introduction

Organic light-emitting diodes (OLEDs) are being investigated extensively for their applications in high-efficiency, low-drive voltage, large-area flat-panel displays.^[1] Particular interest has been focused recently toward phosphorescent OLEDs (PhOLEDs) because of the higher efficiencies resulting from strong spin-orbit coupling effects induced by heavy-metal centers. PhOLEDs employing transition-metal-containing complexes as emitting guests, which are normally dispersed into appropriate host materials, can harvest both singlet and triplet excitons for emission, thereby providing the opportunity to realize internal quantum efficiencies close to 100% (external quantum efficiency (η_{ext}) = ca. 20% (ph/el)).^[2] Transition-metal-centered phosphors with emission colors covering the full visible spectrum have been ob-

tained through varying the structural features of the ligands and the nature of the metal centers (e.g., Ir,^[3] Os,^[4] and Pt^[5]), thereby allowing the realization of full-color PhOLED displays. To obtain high-performance PhOLEDs, the host material must have a triplet energy higher than that of the emitting phosphor, regardless of the emission colors from transition-metal-centered phosphors, thereby preventing detrimental reverse-energy transfer.^[6] In addition, sophisticated device configurations are typically required to facilitate electron/hole injection into the emitting layer (EML) and to confine the emissive exciton efficiently onto the phosphor. Apart from device engineering, the development of tailor-made host compounds that combine various functions into a multifunctional material with balanced hole- and (bipolar) electron-transport properties is another potential alternative approach toward highly efficient PhOLEDs. By hybridizing p- and n-type structural features into a bipolar host material, more-balanced charge fluxes can be achieved with better carrier injection/transport properties in the EML, thus possibly resulting in higher device performance. Although effective bipolar host materials for red, green, and blue phosphors have been reported in recent years,^[7] research directed toward the synthesis of bipolar host materials for red phosphorescence has been rather limited. Chien et al. reported that doping the osmium phosphor [Os(fptz)₂(PPh₂Me)₂] into the host material 2,7-bis(diphenylphosphoryl)-9-[4-(*N,N*-diphenylamino)phenyl]-9-phenylfluorene (POAPF) provided devices with maximum efficiencies as high as 19.9% and 34.5 Lm W⁻¹.^[4a] Ma and co-workers synthesized an oxadiazole/carbazole-based bipolar compound

[a] Dr. S.-Y. Ku, E. Mondal, Prof. K.-T. Wong
Department of Chemistry
National Taiwan University
Taipei 106 (Taiwan)
E-mail: kenwong@ntu.edu.tw

[b] Prof. W.-Y. Hung, C.-W. Chen, S.-W. Yang
Institute of Optoelectronic Sciences
National Taiwan Ocean University
Keelung 202 (Taiwan)
E-mail: wenhung@mail.ntou.edu.tw

[c] Prof. Y. Chi
Department of Chemistry
National Tsing Hua University
300 Hsinchu (Taiwan)

(CzOXD) as the host material; when combined with the iridium complex $[\text{Ir}(\text{2-PyDeCz})_2(\text{acac})]$, it afforded a PhOLED device exhibiting a maximum luminance of 15232 cd m^{-2} and a current efficiency of 20 cd A^{-1} .^[8] Ma and co-workers synthesized an *ortho*-linked oxadiazole/amine-based bipolar compound as the host for the red dopant iridium complex bis(1-phenylisoquinolinolato-*C*²,*N*)iridium-(acetylacetonate) $[(\text{piq})_2\text{Ir}(\text{acac})]$, leading to a deep-red electrophosphorescent device with a value of maximum η_{ext} reaching 18.5%.^[9] Shu and co-workers reported a sulfonyl/triphenylamine-based bipolar host material that, when combined with the dopant tris(1-phenylisoquinolinolato-*C*²,*N*)iridium(III) $[\text{Ir}(\text{piq})_3]$, gave a red PhOLED that had efficiencies of 15.8% and 22.0 Lm W^{-1} .^[10] Ma and co-workers combined a triphenylamine/oxadiazole-based bipolar compound (*o*-TPA-*m*-OXD) as the host with the red emitter $[(\text{piq})_2\text{Ir}(\text{acac})]$ as the dopant to develop a PhOLED device that exhibited a remarkable maximum external quantum efficiency (η_{ext}) of 21.6%.^[11] From the point of view of molecular design, the introduction of an electron-donating moiety onto one of the biphenyl branches of a 9,9'-spirobifluorene core and an electron-withdrawing moiety onto the other biphenyl branch^[12] would lead to a bipolar system.^[13] The energy levels of the highest occupied molecular orbital (HOMO), and lowest unoccupied molecular orbital (LUMO), and the carrier fluxes of the resulting spiro-configured bipolar systems can be modulated by varying the structural features of the donor (D) or acceptor (A) parts independently, thereby making such systems potentially attractive for use as active host materials in PhOLEDs.^[14] In a previous study, we applied a bipolar host—2,7-dicyano-2',7'-bis(diphenylamino)-9,9'-spirobifluorene (D2ACN), configured with appropriately positioned electron-deficient cyano- and electron-rich diphenylamino moieties on the respective biphenyl branches of 9,9'-spirobifluorene—in a simple configuration [indium tin oxide (ITO)/mt-DATA/D2ACN:-(Mpq_2)Ir(acac)/LiF/Al] to give a device with a moderately high value of η_{ext} (10.8%) and a brightness of $23,400 \text{ cd m}^{-2}$.^[15] Although the bipolar character and suitable frontier-orbital energies of D2ACN made it possible to achieve a cost-effective device configuration, this simple device gives lower performance at higher voltages because the absence of neighboring functional layers results in the poor confinement of excitons. To efficiently confine excitons

within the emission layer, it would be necessary to fabricate multilayer devices with the EML incorporating the spiro-configured bipolar host. To optimize the device configuration, it would be desirable to perform a systematic study of the correlation between the physical properties (e.g., triplet energies, energy levels, charge mobility) and the structural features of 9,9'-spirobifluorene-based bipolar compounds. Herein, we report that multilayer PhOLED devices employing those spiro-configured bipolar compounds as hosts doped with green or red dopants can achieve high efficiencies. One of these devices, which adopts D2ACN as the host and $[\text{Os}(\text{bpftz})_2(\text{PPhMe}_2)_2]$ as the emitter, provided a saturated red electrophosphorescence with CIE coordinates (*x*, *y*) of (0.65, 0.35) and remarkably high efficiencies of 20.3% (21 cd A^{-1}) and 13.5 Lm W^{-1} .

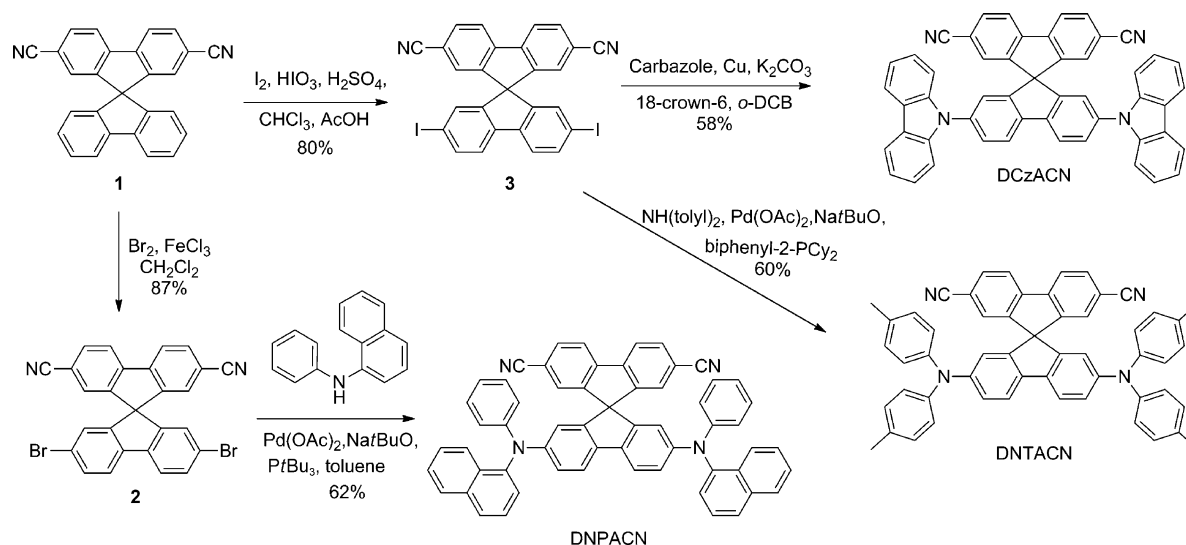
Results and Discussion

The bipolar compounds comprise a cyano-substituted biphenyl branch as an acceptor orthogonally bridged to a donor branch bearing various diarylamino groups. Scheme 1 presents our synthetic routes toward these bipolar hosts, starting from 2,7-dicyano-9,9'-spirobifluorene (**1**).^[15] The dibromination of **1** was achieved through treatment with an excess of Br_2 and a catalytic amount of FeCl_3 to afford the dibromide **2** in 87% yield. Palladium-catalyzed C–N bond formation through cross-coupling of **2** with 1-naphthylphenylamine gave DNPACN (62%). Unfortunately, the palladium-catalyzed C–N bond-formations of the dibromide **2** with di(*para*-tolyl)amine and carbazole failed. Therefore, we introduced more-reactive iodo groups onto compound **1** by reacting with I_2 and HIO_3 in AcOH and CHCl_3 to give 2,2'-diiodo-9,9'-spirobifluorene (**3**) in 80% yield. Subsequent palladium-catalyzed C–N bond-formation through cross-coupling of the diiodospirofluorene **3** with di(*para*-tolyl)amine afforded the bipolar host DNTACN in 60% yield. We isolated the bipolar host DCzACN in a yield of 58% yield through an Ullmann-type copper-mediated cross-coupling of the diiodospirofluorene **3** and carbazole in 1,2-dichlorobenzene.

We used differential scanning calorimetry (DSC) and thermogravimetric analysis (TGA) to characterize the thermal properties of the bipolar host compounds (Table 1). Governed by their molecular weights, the bipolar hosts exhibited glass-transition temperatures (T_g) in the order DNPACN > DNTACN > D2ACN. The rigidity of the donor branch had a great influence on the value of T_g —as exemplified by DCzACN, which exhibited a distinct glass transition at a temperature of 200 °C. Nevertheless, all of these materials formed homogeneous and stable amorphous films, an essential property for OLED device applications. We ascribe the amorphous behavior and high values of T_g to the rigidity of the spirobifluorene core and to the bulk of the diarylamino and carbazole substituents, which effectively suppressed intermolecular interactions. The rigid spirobifluorene skeleton and bulky substituent groups also imparted

Abstract in Chinese:

在這研究中，我們設計合成一系列以旋環雙芴為核心之雙極性分子(D2ACN、DNPACN、DNTACN、DCzACN)。這些雙極性分子是由膾基取代(拉電子基)的聯苯和苯胺基取代(推電子基)的聯苯以 sp^3 混成的碳橋接建構而成。雙極性分子可以藉由取代基的改變調控相穩定性、三重態能階、電子電洞的傳遞及分子的能階(HOMO 和 LUMO)。這類新型分子最大的特點是同時具備傳遞電子和電洞的能力，並擁有相近的載子移動率，此優點可以有效應用在高效能磷光發光二極體。元件的製備是採用多層結構，其中以雙極性分子為主體材料，Ir-綠光錯合物和 Os-紅光錯合物為磷光發光體，此結構特點是能有效局限電子電洞在發光層中結合，並有效阻止激子擴散進而改善元件效率。其中，由 D2ACN 搭配紅光染料 $[\text{Os}(\text{bpftz})_2(\text{PPhMe}_2)_2]$ 的元件可以提供飽合的紅光電致發光(CIE:0.65, 0.35)及高效率 20.3% (21 cd A^{-1})。



Scheme 1. Synthesis of the bipolar host compounds.

Table 1. Physical properties of D2ACN, DNPACN, DNTACN, and DCzACN.

	T_g/T_d [°C]	${}^a E_{1/2}^{Ox}/E_{1/2}^{Red}$ [V]	$\lambda_{abs}/\lambda_{PL}$ [nm] film	E_T [eV]	HOMO/LUMO/ $E_g^{[c]}$ [eV]	μ_h/μ_e^d [cm^2/Vs]
D2ACN	116/350	0.79/−1.61	330, 383/556	2.40	5.4/2.4/3.0	$2.4 \times 10^{-5}/2.2 \times 10^{-5}$
DNPACN	184/395	0.67/−1.62	334, 382/550	2.37	5.3/2.3/3.0	$3 \times 10^{-5}/7.2 \times 10^{-5}$
DNTACN	156/360	0.63/−1.63	329, 388/570	2.38	5.3/2.4/2.9	$2 \times 10^{-5}/2.3 \times 10^{-5}$
DCzACN	200/420	1.37/−1.54	329, 347/469	2.61	5.7/2.4/3.3	$1.9 \times 10^{-5}/1.9 \times 10^{-6}$

[a] Oxidative CV was performed in 1.0 mM CH_2Cl_2 containing 0.1 M TBAF₆; [b] Reductive CV was performed in 1.0 mM THF containing 0.1 M TBAP; [c] Determined through AC2 measurements; LUMO=HOMO+ E_g ; the value of E_g was calculated from the absorption onset of the solid film; [d] Under an electric field (E) of $4.9 \times 10^5 \text{ V cm}^{-1}$. THF=tetrahydrofuran.

these materials with high tolerance toward thermal degradation, as indicated by their high decomposition temperatures (T_d).

We employed cyclic voltammetry (CV) to study the electrochemical behavior of these spirobifluorene-based bipolar compounds (Figure 1, Table 1). With the exception of DCzACN, we observed reversible voltammograms in both the oxidation and reduction scans, which indicated the formation of stable radical cations and anions upon electrochemical redox processes, thus confirming the bipolar character of these spiro-configured D–A compounds. The first oxidation potentials ($E_{1/2}^{Ox}$) of D2ACN, DNPACN, and DNTACN were 0.79, 0.67, and 0.63 V (vs. Ag/AgCl), respectively. We ascribed the slight differences in oxidation potentials to the structural variations in the diarylamino substituents, thereby providing a potential method for tuning the HOMO energy levels. In contrast, DCzACN exhibited an initial oxidation peak at 1.37 V, a value that is much higher than those of diarylamino-substituted derivatives. We assigned this peak to the oxidation of the carbazole moiety. Notably, the radical cations of carbazole can easily undergo rapid dimerization through coupling at their C3 and C6 sites. The carbazole dimer can be readily electrochemically oxidized at 0.85 V.^[16] Because the spiro-configured bipolar compounds D2ACN, DNPACN, and DNTACN are all equipped with a dicyano-substituted biphenyl branch as the

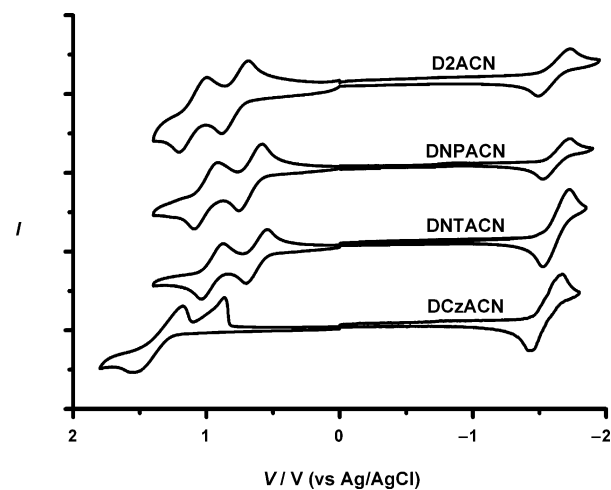


Figure 1. Cyclic voltammograms of D2ACN, DNPACN, DNTACN, and DCzACN.

A unit, they each provided a similar reversible reduction peak near -1.6 V. The electronic nature of the D branch had a slight coulombic repulsion effect on the reduction behavior of the A branch, as evidenced by the lower reduction peak (-1.54 V) of DCzACN, which bears a less-electron-donating carbazole unit on the D branch. Accordingly, modu-

lation of the electronic character or energy levels of these spiro-configured bipolar compounds can be achieved by tuning the structure of the D and/or A branches. We used a photoemission spectrometer (Riken AC-2) to determine the HOMO energy levels of these bipolar compounds, and then estimated their LUMO energy levels from the HOMO energy level and the optical band gaps (E_g) by using the equation $LUMO = HOMO + E_g$. Table 1 summarizes the HOMO and LUMO energies.

Figure 2 presents the absorption and emission spectra of D2ACN, DNPACN, DNTACN, and DCzACN in solid films; Table 1 summarizes the photophysical data. The electronic absorption spectra of D2ACN, DNPACN, and DNTACN are very similar, giving values of λ_{max} near 385 nm, which we attribute to the $\pi-\pi^*$ transitions of the diarylamino-capped biphenyl branches;^[17] in contrast, DCzACN, with its carbazole substituent, exhibited a λ_{max} at 347 nm. The dicyano-substituted biphenyl unit was responsible for an absorption peak at 330 nm. Spiro-configured bipolar compounds typically provide weak emissions from the charge-separated excited state that originates from efficient photoinduced electron transfer.^[15] Consequently, D2ACN, DNPACN, and DNTACN gave very similar photoluminescence (PL) emission maxima, centered at $\lambda_{max} = 560$ nm. In contrast, the spectrum of DCzACN displayed an emission maximum centered at 469 nm, a blue-shift of 90 nm, owing to the weakly electron-donating character of the carbazole unit. From the

highest-energy 0-0 phosphorescence emissions recorded from ethanol solutions at 77 K, we estimated the triplet energies (E_T) of D2ACN, DNPACN, and DNTACN to be approximately 2.4 eV. Notably, the phosphorescence signals of the bipolar compounds D2ACN, DNPACN, and DNTACN were slightly blue-shifted relative to their fluorescence signals. To determine the origin of the phosphorescence of D2ACN, we measured phosphorescence spectra of its individual chromophore components, D2 and ACN (Figure 3). The phosphorescence spectrum of A chromophore ACN

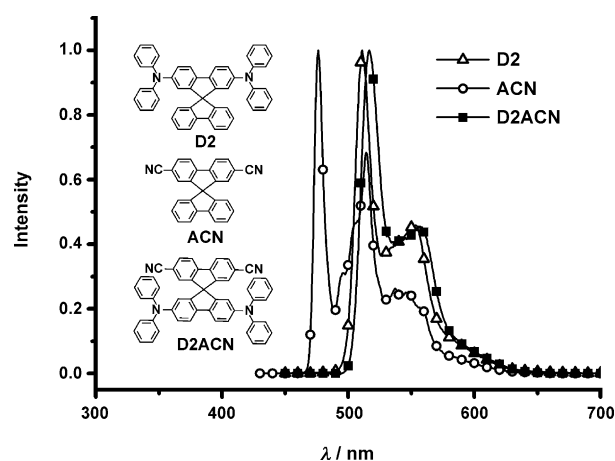


Figure 3. Phosphorescence (Phos) spectra of D2, ACN, and D2ACN recorded from their EtOH solutions at 77 K.

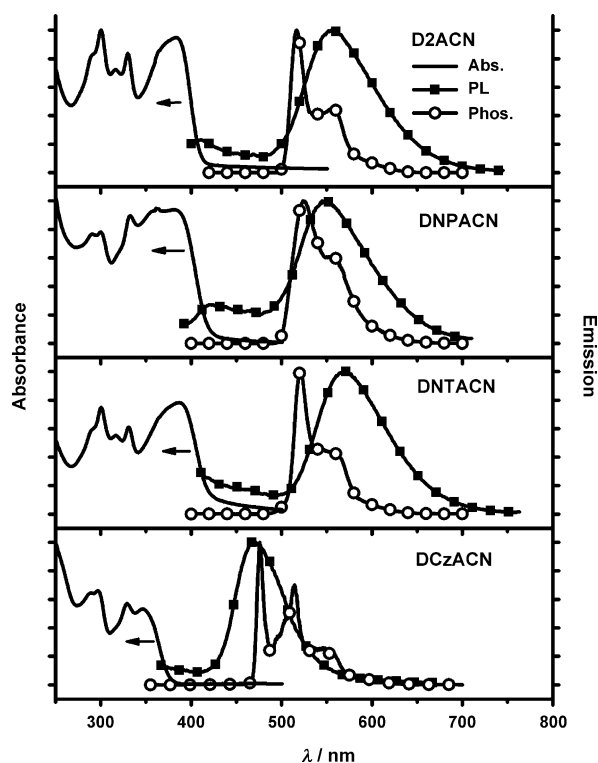


Figure 2. Room-temperature absorption and emission (PL) spectra of D2ACN, DNPACN, DNTACN, and DCzACN in the form of neat films and corresponding phosphorescence (Phos) spectra recorded from their EtOH solutions at 77 K.

featured three emission peaks at 477, 512, and 544 nm, respectively; the D chromophore had a lower-energy triplet state, with phosphorescence signals appearing at 510 and 550 nm, similar to the spectrum of D2ACN. Thus, the phosphorescence of the bipolar compound D2ACN arose from the D chromophore component, which features the lower triplet energy level. The values of E_T of D2ACN, DNPACN, and DNTACN are sufficiently high to confine the triplet excitons of red phosphors. On the other hand, DCzACN, with its higher triplet energy ($E_T = 2.61$ eV), appeared to be a potential host material for green and red triplet emitters.

We employed the time-of-flight (TOF) transient-photocurrent technique^[18] at room temperature to investigate the carrier-transport properties of DNPACN, DNTACN, and DCzACN; we have previously reported the carrier mobility of D2ACN.^[15] Figure 4 displays typical room-temperature TOF transients for these materials under an applied electric field; we observe a nondispersive hole transient photocurrent for DNTACN and dispersive transient photocurrents for the other bipolar compounds. From double-logarithmic representations (Figure 4a-f, insets), we extracted the carrier-transit times (t_T), required to determine the carrier mobilities, from the intersection points of the two asymptotes; we then calculated the mobility using the formula $\mu = d^2/Vt_T$, where d is the sample thickness and V is the applied voltage.

Figure 5 reveals the dependence of the carrier mobilities of these bipolar compounds on the electric field. The hole

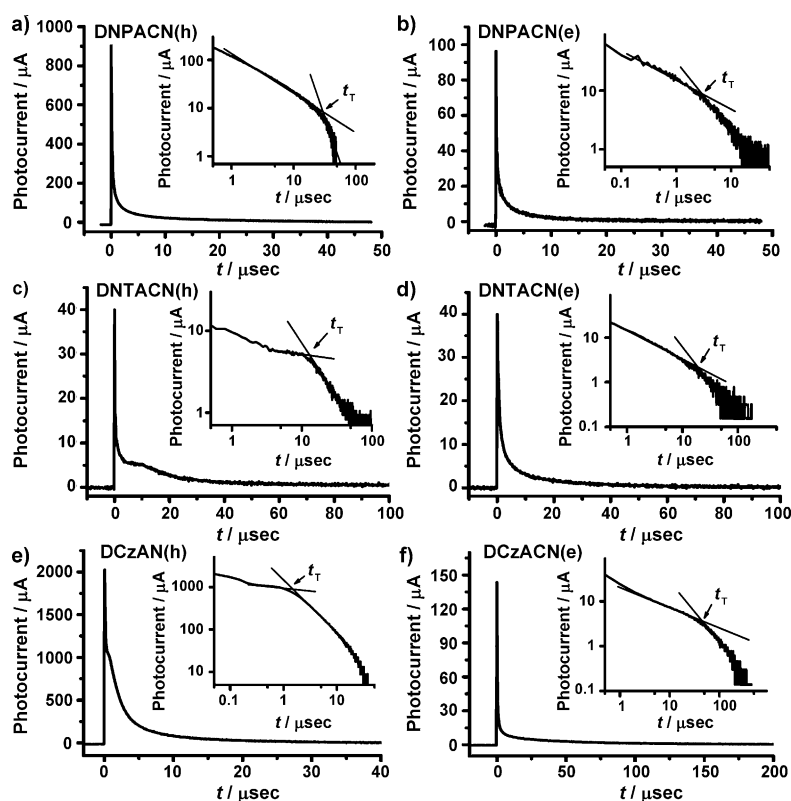


Figure 4. Time-of-flight (TOF) transients of the spirobifluorene-based bipolar compounds: a) DNPACN, hole; $E = 2.3 \times 10^5 \text{ V cm}^{-1}$. b) DNPACN, electron; $E = 4.8 \times 10^5 \text{ V cm}^{-1}$. c) DNTACN, hole; $E = 6 \times 10^5 \text{ V cm}^{-1}$. d) DNTACN, electron; $E = 4.8 \times 10^5 \text{ V cm}^{-1}$. e) DCzACN, hole; $E = 10^6 \text{ V cm}^{-1}$. f) DCzACN, electron; $E = 6.2 \times 10^5 \text{ V cm}^{-1}$.

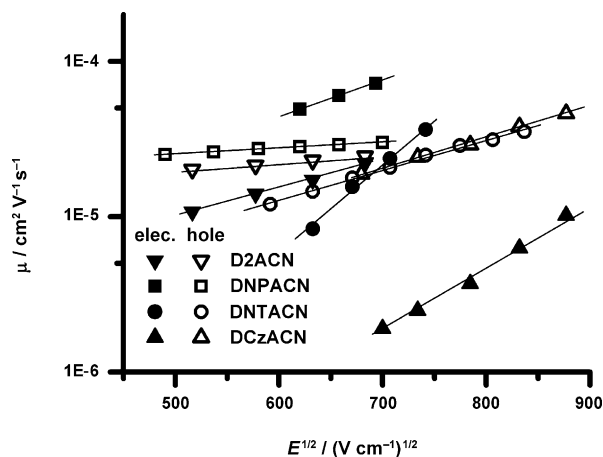


Figure 5. Hole- and electron mobilities for films of D2ACN, DNPACN, DNTACN, and DCzACN plotted with respect to $E^{1/2}$.

mobilities fell within the range $1.2\text{--}4.7 \times 10^{-5} \text{ cm}^2 \text{ V}^{-1} \text{ s}^{-1}$ for fields varying from $2.5\text{--}7.7 \times 10^5 \text{ V cm}^{-1}$; the electron mobilities varied greatly: within the range from 2×10^{-6} to $8 \times 10^{-5} \text{ cm}^2 \text{ V}^{-1} \text{ s}^{-1}$ for fields varying from $2.6\text{--}7.7 \times 10^5 \text{ V cm}^{-1}$. The field-dependence of the carrier mobilities followed the nearly universal Poole–Frenkel relationship $\mu \propto \exp(\beta E^{1/2})$ typically observed for disordered organic systems, where β is

the Poole–Frenkel factor.^[19] By extrapolating the data to the electric field at $4.9 \times 10^5 \text{ V cm}^{-1}$, these compounds all exhibited a similar hole mobility of $2\text{--}3 \times 10^{-5} \text{ cm}^2 \text{ V}^{-1} \text{ s}^{-1}$. Therefore, the different D substituents (diarylamine, carbazole) did not have a pronounced effect on the hole mobility. The films of the spiro-configured bipolar compounds with diarylamino substituents (D2ACN, DNPACN, DNTACN) possessed electron mobilities that followed the same order of their hole mobilities, giving ambipolar charge transport characteristics that should benefit the charge carrier balance in the EML. However, the electron mobility of DCzACN was one order of magnitude lower than those of its diarylamino-substituted counterparts. Presumably, the attachment of different donors (diarylamine or carbazole) onto the spirobifluorene core results in significant differences in the molecular packing. As a consequence, the different internal

reorganization energies and positional disorder, which are critical for carrier transport, will play crucial roles affecting the electron mobility. Nevertheless, bipolar transporting behavior is necessary to maintain charge balance in the emissive layer (EML)—in turn, generating broader recombination zones and steering them away from the interfaces with the neighboring charge-transport layers to suppress emissive exciton quenching.

Because of its ambipolar characteristics and suitable energy levels, we have previously demonstrated the use of D2ACN as a host material for an iridium-based red emitter in a virtual single-layer PhOLED.^[15] To achieve high-efficiency OLEDs, here we adopted a multilayer device structure to facilitate carrier injection, decreased the energy barriers between the interfacial layers, balanced the carrier transport, and confined the excitons within the emissive zone; this device structure was ITO/polyethylenedioxythiophene:polystyrenesulfonate (PEDOT:PSS, 30 nm)/4,4'-bis[*N*-(1-naphthyl)-*N*-phenyl]biphenyldiamine (α -NPD, 20 nm)/4,4',4''-tri(*N*-carbazolyl)triphenylamine (TCTA, 5 nm)/EML (25 nm)/1,3,5-tris(*N*-phenylbenzimidazol-2-yl)benzene (TPBI, 50 nm)/LiF (0.5 nm)/Al (100 nm). This device architecture resembles those reported in the literature,^[20] with PEDOT:PSS and α -NPD functioning as hole-injection and hole-transport layers, respectively. To further improve the efficiency and decrease the hole-injection barri-

er, we inserted a thin layer of TCTA between the NPB layer and the EML to function as both a hole-transporting material and an exciton blocker ($E_T = 2.76$ eV)^[21] preventing diffusion of excitons to the α -NPB layer. TPBI functioned as both a hole-blocking and electron-transporting layer;^[22] LiF was the electron-injection material. Finally, we completed the device by depositing a thin layer of aluminum to serve as the cathode. The EML comprised the bipolar hosts doped with 10 wt % of the red dopants osmium(II) bis[3-(trifluoromethyl)-5-(4-*tert*-butylpyridyl)-1,2,4-triazolate]dimethylphenylphosphine [Os(bpftz)₂(PPhMe₂)₂, OS1]^[23] and osmium(II) bis[3-(trifluoromethyl)-5-(4-*tert*-butylpyridyl)-1,2,4-triazolate]diphenylmethylphosphine [Os(bpftz)₂(PPh₂Me)₂, OS2].^[24] We also inspected the

ability of DCzACN to function as a host in green phosphorescent devices; in this regard, we adopted bis(2-phenylpyridinato)iridium(III) acetylacetonate [(PPy)₂Ir(acac)]^[25] and tris(2-phenylpyridinato)iridium(III) [Ir(PPy)₃]^[26] as dopants. Figure 6 displays the energy levels for the devices and the chemical structures of the heavy-metal complexes. Table 2 summarizes the electroluminescence data obtained from all of the devices.

Figure 7 presents the current-density–voltage–luminance (I – V – L) characteristics, device efficiencies, and EL spectra for the devices incorporating D2ACN, DNPACN, DNTACN, and DCzACN doped with OS1 (devices A1, B1, C1, and D1, respectively). All of the devices in this study exhibited relatively low turn-on voltages (2.5–3.0 V), presumably because of the small energy differences between the

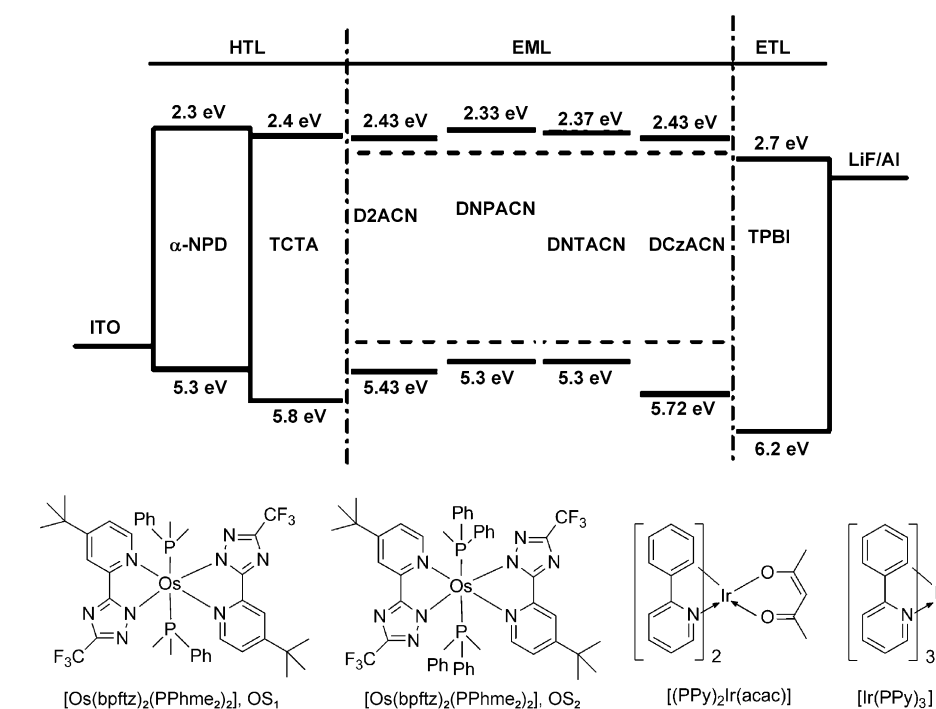


Figure 6. HOMO and LUMO energy levels for the devices and chemical structures of the heavy-metal complexes.

work function of ITO and the HOMO energy levels of the emitters (Figure 6). TPBI served as an effective hole-blocker because of the large differences in the HOMO energies (0.48–0.9 eV) of TPBI and the spirobifluorene derivatives. In contrast, the relatively smaller differences in LUMO energies (0.27–0.37 eV) of TPBI and the spirobifluorene derivatives facilitated injection of electrons from TPBI into the emitter. In Figure 7a, we attribute the differences in the I – V plots of the devices featuring the various hosts to slight differences in the energy level alignments of the devices. The devices that required higher operating voltages (with DNPACN (B1) and DNTACN (C1) as hosts) had higher LUMO energy levels than those of the other devices (using D2ACN (A1) and DCzACN (D1)), thus resulting in impeded flows of electrons. Among the devices, the D2ACN-

Table 2. EL performance of devices incorporating various hosts and emitters.

Emitter ^[a]	$V_{on}^{[b]}$ [V]	L_{1000} nit [V, %]	L_{max} [$cd\ m^{-2}$, V]	I_{max} [$mA\ cm^{-2}$]	η_{ext} [%]	η_c [$cd\ A^{-1}$]	η_p [lm/W]	
A1	D2ACN:OS1	2	5.2, 20.3	134,700, 11	2420	20.4	22.7	21.1
A2	D2ACN:OS2	2	5.1, 19.5	167,200, 12	2740	19.5	27.8	25.6
B1	DNPACN:OS1	2.5	6.1, 16.4	86,300, 12	2110	16.5	15.8	13
B2	DNPACN:OS2	2.5	6.1, 14.9	102,400, 12	1940	15	20.2	14.4
C1	DNTACN:OS1	2	4.9, 15.6	69,200, 12	1610	15.7	17	16.6
C2	DNTACN:OS2	2	4.9, 11.9	72,400, 11	1260	11.9	16.5	15.2
D1	DCzACN:OS1	2.5	5.5, 16.7	84,400, 11.5	3080	17.7	21.4	16.3
D2	DCzACN:OS2	2.5	5.6, 19.2	113,000, 12	2540	19.3	31.9	22.4
D3	DCzACN:Ppy2	2.5	4.9, 12	66,800, 12.5	980	12.6	46	44.3
D4	DCzACN:Ppy3	2.5	5, 8.8	29,000, 12.5	1100	10.7	32.4	32

[a] Device configuration: ITO/PEDOT:PSS/ α -NPB (20 nm)/TCTA (5 nm)/host:dopant 10 wt % (25 nm)/TPBI (50 nm)/LiF/Al. [b] Turn-on voltage at which emission became detectable (10^{-2} $cd\ m^{-2}$).

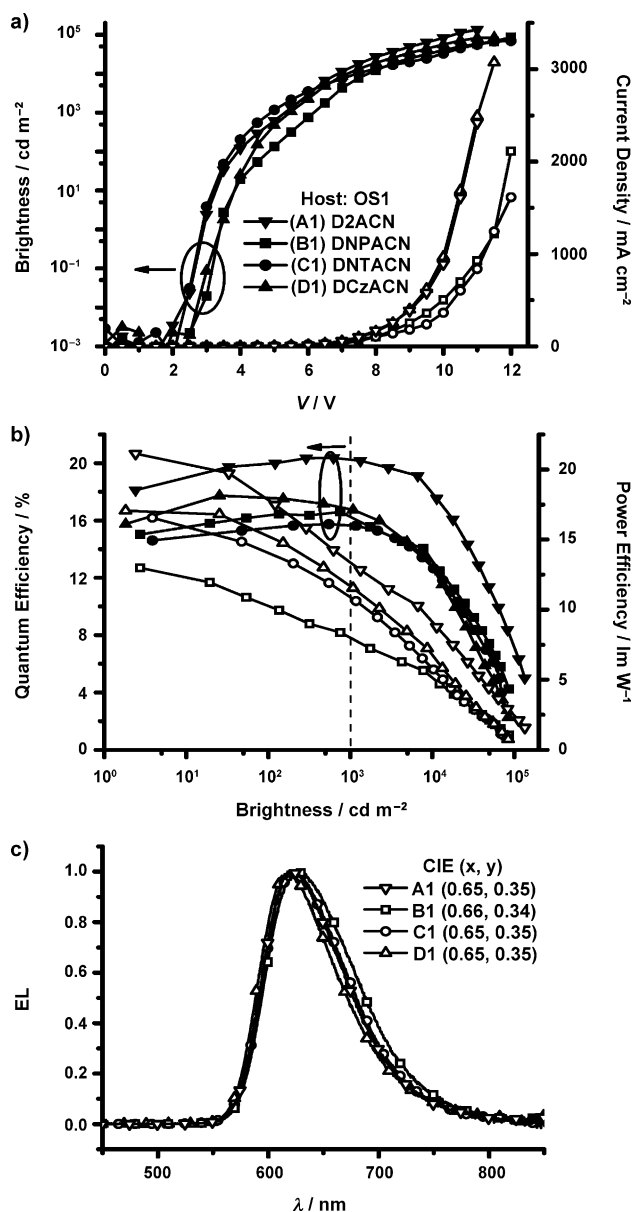


Figure 7. a) I - V - L characteristics, b) plots of EL efficiency with respect to brightness, and c) EL spectra for devices incorporating hosts doped with OS1.

based device A1 exhibited a relatively high brightness of $134,700 \text{ cd m}^{-2}$, driven at a current density of 2420 mA cm^{-2} (11 V). Figure 7b displays the external quantum efficiencies (η_{ext}) and power efficiencies (η_{p}) of the devices, plotted with respect to the luminance. The maximum values of η_{ext} and η_{p} for device A1 (20.4% and 21.1 lm W^{-1} , respectively) were greater than those of devices B1 (16.5% and 13 lm W^{-1} , respectively), C1 (15.7% and 16.6 lm W^{-1} , respectively), and D1 (17.7% and 16.3 lm W^{-1} , respectively). The value of η_{ext} for device A1 of 20.4% is at the theoretical limit of 20% for phosphorescent OLEDs. Notably, even when the brightness reached 1000 cd m^{-2} , the external quantum efficiency (η_{ext}) of device A1 remained at 20.3%, thus

indicating balanced injection and transport of holes and electrons in the device, even at high current densities.

These results also reveal that a bipolar host material can provide balanced charge fluxes within the EML, rendering devices exhibiting only a limited external quantum efficiency roll-off. The performance of device A1 is comparable with the previously reported highest values for red PhOLEDs.^[4a,27] In Figure 7c, we find that the features in the EL spectra of devices resulted only from the red emission of $[\text{Os}(\text{bpftz})_2(\text{PPhMe}_2)_2]$, thus indicating that TCTA and TPBI functioned as effective blockers to confine carriers and excitons within the EML. Figure 8 displays the behavior of the corresponding OS2-based devices. The best performance was also that for the D2ACN-based device A2,

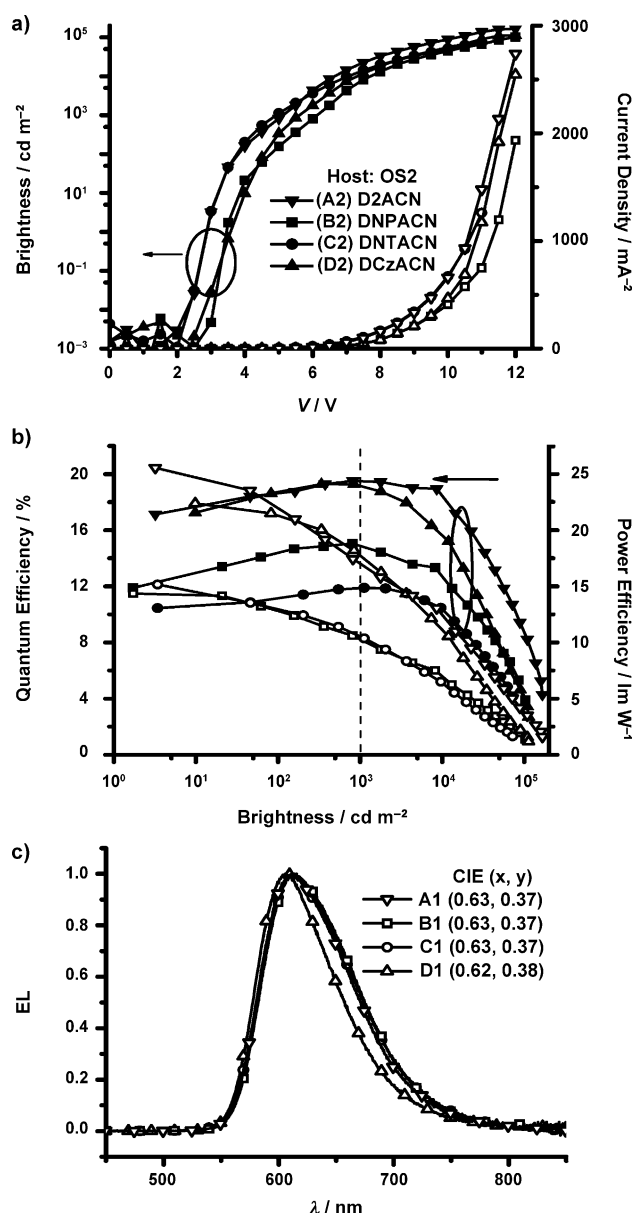


Figure 8. a) I - V - L characteristics, b) plots of EL efficiency with respect to brightness, and c) EL spectra for devices incorporating hosts doped with OS2.

which exhibited saturated red emission CIE(x,y)=0.63,0.37 with maximum brightness, external quantum efficiency (η_{ext}), and power efficiency (η_{p}) of 167,200 cd m^{-2} , 19.5%, and 25.6 Lm W^{-1} , respectively.

To test the ability of DCzACN ($E_{\text{T}}=2.61$ eV) to function as a host material for green phosphorescent devices, we incorporated [(PPy)₂Ir(acac)] and [Ir(PPy)₃] as dopants in devices D3 and D4 having the same device configuration as that described above. Figure 9 reveals that device D3 exhibited a maximum brightness (L_{max}) of 66,800 cd m^{-2} at 12.5 V and a maximum external quantum efficiency (η_{ext}) of 12.6%; device D4 provided a maximum brightness (L_{max}) of 29,000 cd m^{-2} at 12.5 V and a maximum external quantum efficiency (η_{ext}) of 10.7%. These results suggest that our

present device structure, incorporating DCzACN as a bipolar host, generally provides highly efficient OLEDs for both red and green phosphors.

Conclusions

We have synthesized and characterized a series of spirobi-fluorene-based bipolar compounds (D2ACN, DNPACN, DNTACN, DCzACN), and tailored the morphological stability, triplet energy (E_{T}), bipolar charge-transport behavior, and HOMO/LUMO energy levels by independently varying the structural features of the D and A branches. Efficient photoinduced electron transfer resulted in the bipolar compounds D2ACN, DNPACN, and DNTACN, which have low-lying excited states. Interestingly, the phosphorescence originating from the D branches was located at higher energy relative to the charge-separated singlet emissions. The physical properties of these new compounds—most importantly, their balanced electron and hole mobilities—make them useful as host materials for high-efficiency phosphorescent OLEDs. We fabricated multilayer devices employing these new host materials, doped with iridium-based green or osmium-based red phosphors, as the EML. This multilayer structure efficiently confines holes and electrons within the EML and prevents exciton diffusion, offering higher device efficiencies. One of these devices, incorporating D2ACN doped with the red emitter [Os(bpftz)₂(PPhMe₂)₂], exhibited saturated red electrophosphorescence with CIE coordinates (x, y) of (0.65, 0.35) and remarkably high efficiencies of 20.3% (21 cd A^{-1}) and 13.5 Lm W^{-1} at a practical brightness of 1000 cd m^{-2} .

Experimental Section

Cyclic Voltammetry

The oxidation potentials were determined in CH_2Cl_2 solutions (1.0 mM) containing 0.1 M tetra-*n*-butylammonium hexafluorophosphate (TBAPF₆) as the supporting electrolyte at a scan rate of 100 mV s^{-1} . The reduction potentials were determined in THF solutions (1.0 mM) containing 0.1 M tetra-*n*-butylammonium perchlorate (TBAP). A glassy carbon electrode and a platinum wire were used as the working and counter electrodes, respectively. All potentials were recorded versus Ag/AgCl (saturated) as a reference electrode. The ferrocenium/ferrocene redox couple in THF/TBAP occurs at a value of $E_{\text{o}}' = +0.61$ V for oxidation and in CH_2Cl_2 /TBAPF₆ at +0.45 V for reduction, with respect to Ag/AgCl (saturated).

Synthetic Procedures

Spiro-compound 3

A mixture of **1** (7.32 g, 20.00 mmol), I₂ (6.88 g, 27.20 mmol), iodic acid (1.65 g, 9.40 mmol), concentrated H₂SO₄ (2 mL), and CHCl₃ (20 mL) in AcOH (80 mL) was heated at 60 °C for 12 h. After cooling to room temperature, the mixture was partitioned between CHCl₃ and H₂O and the organic phase was washed with H₂O and NaHCO₃(aq.). The organic phase was collected, dried (MgSO₄), and the crude product was purified by column chromatography on silica gel to give a white powder (9.88 g, 80%). $R_{\text{T}}=0.33$ (EtOAc/hexanes); m.p.: 373 °C (DSC); IR (KBr): $\tilde{\nu}=825, 932, 999, 1378, 1444, 1603, 2217$ cm^{-1} ; ¹H NMR (400 MHz, CDCl₃, 25 °C): $\delta=7.99$ (dd, ³ $J_{\text{H,H}}=8.0, ^5J_{\text{H,H}}=0.8$ Hz, 2H), 7.78 (dd, ³ $J_{\text{H,H}}=6.4,$

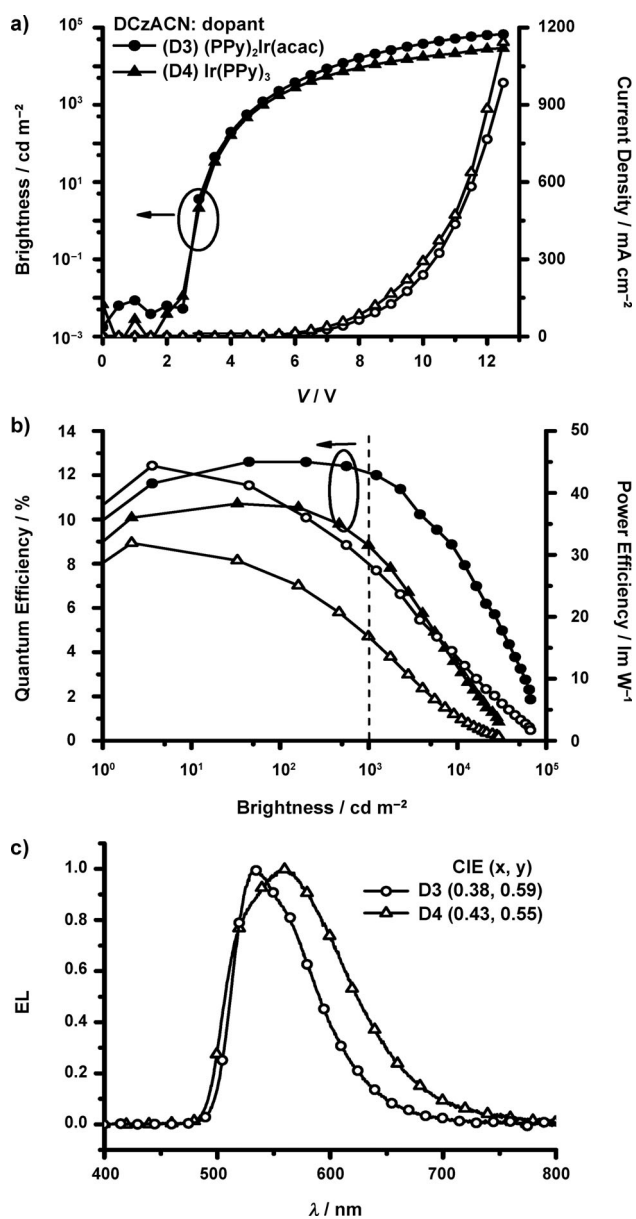


Figure 9. a) I - V - L characteristics, b) plots of EL efficiency with respect to brightness, and c) EL spectra for devices incorporating DCzACN doped with green phosphors.

$^4J_{\text{HH}}=1.2$ Hz, 2H), 7.76 (dd, $^3J_{\text{HH}}=6.0$, $^4J_{\text{HH}}=1.6$ Hz, 2H), 7.61 (d, $^3J_{\text{HH}}=8.0$ Hz, 2H), 7.05 (d, $^4J_{\text{HH}}=0.8$ Hz, 2H), 6.94 ppm (d, $^4J_{\text{HH}}=1.2$ Hz, 2H); ^{13}C NMR (100 MHz, CDCl_3 , 25 °C): $\delta=148.6$, 147.0, 143.7, 140.3, 138.1, 133.0, 132.9, 132.7, 128.0, 122.3, 122.0, 121.9, 118.1, 113.1, 93.9, 64.8, 53.4 ppm; MS (FAB⁺) m/z (%) 617.9 (100); HRMS calcd for $\text{C}_{27}\text{H}_{12}\text{I}_2\text{N}_2$: 617.9090; found: 617.9066.

DNPACN

$\text{Pd}(\text{OAc})_2$ (0.02 g, 0.09 mmol), *N*-phenylnaphthalen-1-amine (1.32 g, 6.00 mmol), *t*BuONa (1.15 g, 12.00 mmol), and **1** (1.05 g, 2.00 mmol) were placed in a 50 mL two-neck flask fitted with a septum. The flask was evacuated and back-filled with argon. Toluene (15 mL) and PrBu_3 (0.05 mL in toluene, 4 mL, 0.20 mmol) were added via a syringe at room temperature. The reaction mixture was heated at 110 °C for 2 days before being cooled to room temperature and quenched with water (20 mL). The aqueous phase was extracted with CH_2Cl_2 (3×15 mL). The combined organic phases were dried (MgSO_4) and concentrated to obtain DNPACN (980 mg, 64%), which was purified by column chromatography on silica gel. $R_f=0.50$ (EtOAc/hexanes); m.p. > 400 °C (DSC); IR (KBr): $\tilde{\nu}=778$, 1270, 1383, 1465, 1490, 1588, 2223 cm^{-1} ; ^1H NMR (400 MHz, CDCl_3 , 25 °C): $\delta=7.77$ – 7.74 (m, 4H), 7.67– 7.62 (m, 6H), 7.52– 7.49 (m, 4H), 7.39 (t, $^3J_{\text{HH}}=7.6$ Hz, 2H), 7.35– 7.27 (m, 4H), 7.15 (d, $^3J_{\text{HH}}=7.6$ Hz, 2H), 7.07– 7.04 (m, 4H), 6.94 (dd, $^3J_{\text{HH}}=8.4$, $^4J_{\text{HH}}=2.0$ Hz, 2H), 6.87– 6.82 (m, 6H), 6.22 ppm (d, $^4J_{\text{HH}}=1.2$ Hz, 2H); ^{13}C NMR (100 MHz, CDCl_3 , 25 °C): $\delta=168.3$, 150.3, 149.6, 147.8, 147.6, 146.9, 144.1, 143.0, 142.8, 135.3, 134.8, 133.5, 131.5, 130.2, 128.8, 128.0, 127.3, 127.2, 126.4, 126.4, 126.0, 125.9, 123.9, 123.0, 122.0, 121.9, 121.7, 121.1, 121.0, 118.8, 116.8, 111.2, 110.4, 65.4 ppm; elemental analysis: calcd (%) for $\text{C}_{59}\text{H}_{36}\text{N}_4$: C 88.47, H 4.53, N 7.00; found: C 88.19, H 4.62, N 6.41.

DNTACN

Using the procedure described above, a mixture of $\text{Pd}(\text{OAc})_2$ (0.02 g, 0.09 mmol), di-*para*-tolylamine (0.68 g, 3.50 mmol), *t*BuONa (0.38 g, 3.95 mmol), 1-biphenyldicyclohexylphosphine (0.050 g, 0.15 mmol), and **3** (0.93 g, 1.50 mmol) was heated at 110 °C for 24 h to yield DNTACN (680 mg, 56%), which was purified by column chromatography on silica gel. $R_f=0.33$ (CH_2Cl_2 /hexanes); m.p.: 313 °C (DSC); IR (KBr): $\tilde{\nu}=809$, 1265, 1465, 1506, 1598, 2217 cm^{-1} ; ^1H NMR (400 MHz, CDCl_3 , 25 °C): $\delta=7.80$ (d, $^3J_{\text{HH}}=8.0$ Hz, 2H), 7.65 (dd, $^3J_{\text{HH}}=8.0$, $^4J_{\text{HH}}=1.2$ Hz, 2H), 7.54 (d, $^3J_{\text{HH}}=8.4$ Hz, 2H), 7.20 (d, $^4J_{\text{HH}}=0.8$ Hz, 2H), 7.96– 7.93 (m, 10H), 6.83 (d, $^3J_{\text{HH}}=8.4$ Hz, 8H), 6.32 (d, $^4J_{\text{HH}}=2.0$ Hz, 2H), 2.24 ppm (s, 12H); ^{13}C NMR (100 MHz, CDCl_3 , 25 °C): $\delta=150.6$, 147.6, 146.3, 145.0, 143.8, 135.5, 132.4, 132.0, 129.7, 127.8, 124.0, 123.7, 121.8, 120.3, 118.6, 117.9, 112.3, 65.4, 10.7 ppm; MS (FAB⁺) m/z (%) 756.8 (100); HRMS calcd for $\text{C}_{59}\text{H}_{36}\text{N}_4$: 756.3253; found: 756.3245; elemental analysis: calcd (%) for $\text{C}_{55}\text{H}_{40}\text{N}_4$: C 87.27, H 5.33, N 7.40; found: C 87.33, H 5.36, N 7.29.

DCzACN

A mixture of **3** (2.47 g, 4.00 mmol), carbazole (1.47 g, 8.80 mmol), Cu (0.50 g, 8.00 mmol), K_2CO_3 (1.36 g, 12.00 mmol), and [18]crown-6 (0.21 g, 0.80 mmol) in 1,2-dichlorobenzene (60 mL) was heated under reflux at 185 °C under argon for 2.5 days. The reaction mixture was filtered and the filtrate concentrated under reduced pressure. The crude product was purified by column chromatography on silica gel to give a white solid (1.60 g, 58%). $R_f=0.33$ (CH_2Cl_2 /hexanes); m.p.: 420 °C (DSC); IR (KBr): $\tilde{\nu}=819$, 1229, 1326, 1439, 1495, 1598, 2217 cm^{-1} ; NMR (400 MHz, CDCl_3 , 25 °C): $\delta=8.20$ (d, $^3J_{\text{HH}}=8.0$ Hz, 2H), 8.10 (d, $^3J_{\text{HH}}=7.2$, Hz, 4H), 7.92 (dd, $^3J_{\text{HH}}=8.0$, $^5J_{\text{HH}}=0.8$ Hz, 2H), 7.76 (dd, $^3J_{\text{HH}}=6.8$, $^4J_{\text{HH}}=1.6$ Hz, 4H), 7.40– 7.36 (m, 6H), 7.29– 7.24 (m, 8H), 6.93 ppm (d, $^4J_{\text{HH}}=1.6$ Hz, 2H); ^{13}C NMR (100 MHz, CDCl_3 , 25 °C): $\delta=149.0$, 147.5, 143.7, 140.2, 139.8, 137.8, 132.7, 127.8, 127.6, 125.9, 123.2, 122.3, 122.0, 121.9, 120.2, 120.1, 118.2, 112.9, 109.3, 65.5 ppm; MS (FAB⁺) m/z (%) 696.2 (100); HRMS calcd for $\text{C}_{51}\text{H}_{28}\text{N}_4$: 696.2314; found: 696.2325; elemental analysis: calcd (%) for $\text{C}_{51}\text{H}_{28}\text{N}_4$: C 87.91, H 8.04, N 8.04; found: C 87.95, H 4.13, N 8.02.

Photophysical Measurements

Steady-state spectra were recorded for both the solutions and solid films prepared through vacuum (2×10^{-6} torr) deposition on a quartz plate (1.6×1.0 cm). Absorption spectra were recorded using a U2800 A spectrophotometer (Hitachi). Fluorescence spectra were recorded at 300 K and phosphorescence spectra at 77 K using a Hitachi F-4500 spectrophotometer, with excitation at the absorption maxima. Quantum efficiencies were recorded using an integration sphere coupled with a photonic multi-channel analyzer (Hamamatsu C9920), which gave anthracene a quantum yield of 23%. The experimental HOMO energy levels were determined using a Riken AC-2 photoemission spectrometer (PES); the LUMO energy levels were estimated by subtracting the optical energy gap from the measured HOMO energy level.

TOF Mobility Measurements

The samples for the TOF measurements were prepared through vacuum deposition in the configuration glass/Ag (30 nm)/organic (2–3 μm)/Al (150 nm); they were then placed inside a cryostat and maintained under vacuum. The thickness of the organic film was monitored in situ with a quartz crystal sensor and calibrated through thin-film thickness measurement (K-MAC ST2000). A pulsed nitrogen laser, used as the excitation light source through the transparent electrode (ITO), induced photogeneration of a thin sheet of excess carriers. Under an applied dc bias, the transient photocurrent was swept across the bulk of the organic film toward the collection electrode (Al) and then recorded using a digital storage oscilloscope. Depending on the polarity of the applied bias, selected carriers (holes or electrons) were swept across the sample with a transit time of t_T . With an applied bias V , a sample thickness D , and an applied electric field E equal to V/D , the carrier mobility was given using the formula

$$\mu = D / (t_T E) = D^2 / (V t_T)$$

from which the carrier transit time, t_T , was extracted from the intersection point of two asymptotes to the plateau and the tail sections in double-logarithmic plots.

OLED Device Fabrications

All chemicals were purified by vacuum sublimation prior to use. The OLEDs were fabricated through vacuum deposition of the materials at 10^{-6} torr onto ITO-coated glass substrates that have a sheet resistance of $15 \Omega \text{sq}^{-1}$. The ITO surface was cleaned ultrasonically—sequentially with acetone, methanol, and deionized water—and then it was treated with UV-ozone. A hole-injection layer (PEDOT:PSS) was spin-coated onto the substrates and dried at 130 °C for 30 min to remove residual water. Organic layers were then vacuum-deposited at a deposition rate of ca. 1 – 2 \AA s^{-1} . Subsequently, LiF was deposited at 0.1 \AA s^{-1} and then capped with Al (ca. 5 \AA s^{-1}) through shadow masking without breaking the vacuum. The *I*-*V*-*L* characteristics of the devices were measured simultaneously using a Keithley 6430 source meter and a Keithley 6487 picoammeter equipped with a calibration silicon-photodiode in a glove box. EL spectra were measured using a photodiode array (OTO SD1000) with a spectral range from 300 to 1100 nm and a resolution of 1.5 nm.

Acknowledgements

This study was supported financially by the National Science Council of Taiwan.

- [1] C. W. Tang, S. A. VanSlyke, C. H. Chen, *J. Appl. Phys.* **1989**, *65*, 3610.
- [2] M. A. Baldo, D. F. O'Brien, Y. You, A. Shoustikov, S. Sibley, M. E. Thompson, S. R. Forrest, *Nature* **1998**, *395*, 15.

- [3] a) S. Lamansky, P. Djurovich, D. Murphy, F. Abdel-Razzaq, R. Kwong, I. Tsyba, M. Bortz, B. Mui, R. Bau, M. E. Thompson, *Inorg. Chem.* **2001**, *40*, 1704; b) P. J. Hay, *J. Phys. Chem. A* **2002**, *106*, 1634; c) I. Avilov, P. Minoofar, J. Cornil, L. De Cola, *J. Am. Chem. Soc.* **2007**, *129*, 8247; d) K. Dedeian, P. I. Djurovich, F. O. Garces, G. Carlson R. J. Watts, *Inorg. Chem.* **1991**, *30*, 1685.
- [4] a) C.-H. Chien, F.-M. Hsu, C.-F. Shu, Y. Chi, *Org. Electron.* **2009**, *10*, 871; b) Y. Zhang, F. Huang, A. K.-Y. Jen, Y. Chi, *Appl. Phys. Lett.* **2008**, *92*, 063303; c) F. Huang, P.-I. Shih, C.-F. Shu, Y. Chi, A. K.-Y. Jen, *Adv. Mater.* **2009**, *21*, 361.
- [5] a) X. Yang, Z. Wang, S. Madakuni, J. Li, G. E. Jabbour, *Adv. Mater.* **2008**, *20*, 2405; b) B. Ma, P. I. Djurovich, S. Garon, B. Alleyne, M. E. Thompson, *Adv. Funct. Mater.* **2006**, *16*, 2438.
- [6] M. Sudhakar, P. I. Djurovich, T. E. Hogen-Esch, M. E. Thompson, *J. Am. Chem. Soc.* **2003**, *125*, 7796.
- [7] a) S.-J. Su, H. Sasabe, T. Takeda, J. Kido, *Chem. Mater.* **2008**, *20*, 1691; b) F.-M. Hsu, C.-H. Chien, C.-F. Shu, C.-H. Lai, C.-C. Hsieh, K.-W. Wang, P.-T. Chou, *Adv. Funct. Mater.* **2009**, *19*, 2834; c) S. O. Jeon, K. S. Yook, C. W. Joo, J. Y. Lee, *Adv. Mater.* **2010**, *22*, 1872; d) L.-C. Chi, W.-Y. Hung, H.-C. Chiu, K.-T. Wong, *Chem. Commun.* **2009**, 3892; e) X. Gu, H. Zhang, T. Fei, B. Yang, H. Xu, Y. Ma, X. Liu, *J. Phys. Chem. A* **2010**, *114*, 965; f) H.-H. Chou, C.-H. Cheng, *Adv. Mater.* **2010**, *22*, 2468; g) Y. Tao, C. Yang, J. Qin, *Chem. Soc. Rev.* **2011**, *40*, 2943.
- [8] Y. Tao, Q. Wang, C. Yang, K. Zhang, Q. Wang, T. Zou, J. Qin, D. Ma, *J. Mater. Chem.* **2008**, *18*, 4091.
- [9] Y. Tao, Q. Wang, C. Yang, Q. Wang, Z. Zhang, T. Zou, J. Qin, D. Ma, *Angew. Chem.* **2008**, *120*, 8224; *Angew. Chem. Int. Ed.* **2008**, *47*, 8104.
- [10] F.-M. Hsu, C.-H. Chien, Y.-J. Hsieh, C.-H. Wu, C.-F. Shu, S.-W. Liu, C.-T. Chen, *J. Mater. Chem.* **2009**, *19*, 8002.
- [11] Y. Tao, Q. Wang, L. Ao, C. Zhong, J. Qin, C. Yang, D. Ma, *J. Mater. Chem.* **2010**, *20*, 1759.
- [12] T. P. I. Saragi, T. Spehr, A. Siebert, T. Fuhrmann-Lieker, J. Salbeck, *Chem. Rev.* **2007**, *107*, 1011.
- [13] a) Y.-Y. Chien, K.-T. Wong, P.-T. Chou, Y.-M. Cheng, *Chem. Commun.* **2002**, 2874; b) K.-T. Wong, S.-Y. Ku, Y.-M. Cheng, X.-Y. Lin, Y.-Y. Hung, S.-C. Pu, P.-T. Chou, G.-H. Lee, S.-M. Peng, *J. Org. Chem.* **2006**, *71*, 456.
- [14] a) M.-Y. Lai, C.-H. Chen, W.-S. Huang, J. T. Lin, T.-H. Ke, L.-Y. Chen, M.-H. Tsai, C.-C. Wu, *Angew. Chem.* **2008**, *120*, 591; *Angew. Chem. Int. Ed.* **2008**, *47*, 581; b) Y.-L. Liao, C.-Y. Lin, K.-T. Wong, T.-H. Hou, W.-Y. Hung, *Org. Lett.* **2007**, *9*, 4511; c) C.-H. Chen, W.-S. Huang, M.-Y. Lai, W.-C. Tsao, J. T. Lin, Y.-H. Wu, T.-H. Ke, L.-Y. Chen, C.-C. Wu, *Adv. Funct. Mater.* **2009**, *19*, 2661; d) C.-C. Chi, C.-L. Chiang, S.-W. Liu, H. Yueh, C.-T. Chen, C.-T. Chen, *J. Mater. Chem.* **2009**, *19*, 5561.
- [15] W.-Y. Hung, T.-C. Tsai, S.-Y. Ku, L.-C. Chi, K.-T. Wong, *Phys. Chem. Chem. Phys.* **2008**, *10*, 5822.
- [16] a) S. H. Hosseini, A. A. Entezami, *J. Appl. Polym. Sci.* **2003**, *90*, 63; b) K. M. Omer, S.-Y. Ku, Y.-C. Chen, K.-T. Wong, A. J. Bard, *J. Am. Chem. Soc.* **2010**, *132*, 10944.
- [17] K.-T. Wong, C.-F. Wang, C. H. Chou, Y. O. Su, G.-H. Lee, S.-M. Peng, *Org. Lett.* **2002**, *4*, 4439.
- [18] P. M. Borsenberger, D. S. Weiss in *Organic Photoreceptors for Imaging Systems*, Marcel Dekker, New York, **1993**, and references therein.
- [19] a) W. D. Gill, *J. Appl. Phys.* **1972**, *43*, 5033; b) H. Bässler, *Philos. Mag. B* **1992**, *65*, 795; c) H. Bässler, *Int. J. Mod. Phys. B* **1994**, *8*, 847.
- [20] a) T.-C. Tsai, W.-Y. Hung, L.-C. Chi, K.-T. Wong, C.-C. Hsieh, P.-T. Chou, *Org. Electron.* **2009**, *10*, 158; b) H.-F. Chen, S.-J. Yang, Z.-H. Tsai, W.-Y. Hung, T.-C. Wang, K.-T. Wong, *J. Mater. Chem.* **2009**, *19*, 8112.
- [21] a) S.-J. Su, E. Gonmori, H. Sasabe, J. Kido, *Adv. Mater.* **2008**, *20*, 4189; b) Y.-Y. Lyu, J. Kwak, W. S. Jeon, Y. Byun, H. S. Lee, D. Kim, C. Lee, K. Char, *Adv. Funct. Mater.* **2009**, *19*, 420.
- [22] S.-J. Yeh, M.-F. Wu, C.-T. Chen, Y.-H. Song, Y. Chi, M.-H. Ho, S.-F. Hsu, C. H. Chen, *Adv. Mater.* **2005**, *17*, 285.
- [23] Y.-L. Tung, S.-W. Lee, Y. Chi, Y.-T. Tao, C.-H. Chien, Y.-M. Cheng, P.-T. Chou, S.-M. Peng, C.-S. Liu, *J. Mater. Chem.* **2005**, *15*, 460.
- [24] P.-I. Shih, C.-F. Shu, Y.-L. Tung, Y. Chi, *Appl. Phys. Lett.* **2006**, *88*, 251110.
- [25] C. Adachi, M. A. Baldo, M. E. Thompson, S. R. Forrest, *J. Appl. Phys.* **2001**, *90*, 5048.
- [26] a) H. Inomata, K. Goushi, T. Masuko, T. Konno, T. Imai, H. Sasabe, J. J. Brown, C. Adachi, *Chem. Mater.* **2004**, *16*, 1285; b) X. Ren, J. Li, R. J. Holmes, P. I. Djurovich, S. R. Forrest, M. E. Thompson, *Chem. Mater.* **2004**, *16*, 4743.
- [27] W. S. Jeon, T. J. Park, S. Y. Kim, R. Pode, J. Jang, J. H. Kwon, *Org. Electron.* **2009**, *10*, 240.

Received: May 18, 2011

Published online: October 13, 2011